COMMUNICATION

Check for updates

Grafting self-immolative poly(benzyl ether)s toward sustainable adhesive thermosets with reversible bonding and triggered de-bonding capabilities†

Byeongjun Choi,[a] Ji Woo Kim,[a] Geunyoung Choi,[a] Songah Jeong,[a] Eunpyo Choi [ID][bc] and Hyungwoo Kim [ID] *[a]

This paper demonstrates a molecular design concept for stimuli-responsive polymer adhesives. Self-immolative poly(benzyl ether) (PBE) is synthesized as a functional macro-monomer that provides multiple reversible cross-linking points and autonomously depolymerizes in response to a specific stimulus. Grafting only 0.1 mol% PBE onto a soft polynorbornene matrix leads to the fabrication of an adhesive thermoset that not only acts as a high-shear pressure-sensitive adhesive but is also reusable and readily removable when no longer required. This concept can be refined and realized by tailoring the composition of the monomer, including other functions, or incorporating a diverse range of polymeric structures to produce sustainable applications for practical use.

Stimuli-responsive polymer adhesives that can change their adhesive properties in response to external stimuli have recently become a significant focus of attention.[1–3] In order to be able to adapt to their surroundings or behave as required for specific applications, this class of adhesive requires both the reversible modulation of their adhesive strength and irreversible release behavior in response to specific stimuli such as heat, pH, light, electric and magnetic fields, ultrasound, and/or chemical triggers.[1] In doing so, stimuli-responsive adhesives can be used to overcome the limitations of conventional adhesives, such as their one-time use, difficult removal, and low reusability, and to develop novel platforms such as smart electronics or implantable devices.[4–6]

However, combining both characteristics for the control of adhesive strength without damaging the reliability of these

adhesives remains challenging. In terms of molecular design, a variety of polymeric structures embedded with independent functional moieties that can be orthogonally activated to achieve the desired properties have been proposed. Recent studies have employed dynamic bond exchange,[7–16] isomerization,[17–19] or elimination[15,20,21] for the covalent control of adhesive performance, while non-covalent interactions such as multiple hydrogen bonds or metal coordination have also been used.[6,22–25] However, in most cases, the covalent and non-covalent bonds individually function for adhesive properties so it is difficult to achieve rapid and comprehensive control for them; thus, persistent and/or excessive stimulation is often required, which weakens the energy-efficient re-bonding and/or de-bonding behavior of the adhesive. Despite this, a number of stimuli-responsive and biomimetic polymers have been demonstrated to date,[26–28] thus opening a route to improving these adhesives and expanding their range of applications.

Self-immolative polymers (SIPs), which are a privileged class of low-ceiling-temperature polymers capable of exhibiting autonomous and complete depolymerization in response to external stimuli.[29] They can depolymerize rapidly with directivity and their reaction can be fine-tuned on a molecular level, which is in contrast to degradable polymers with labile backbones that undergo random, repetitive depolymerization reactions such as hydrolysis and biodegradation. In addition to their unique, tunable disassembly behavior, SIPs can induce and/or amplify *in situ* physicochemical changes in materials, thus they have been incorporated into various polymeric architectures[30–33] for a range of bio-related and/or sustainable applications, including diagnosis, sensing, and drug delivery.[34,35] However, they have rarely been used in stimuli-responsive adhesives.

One class of SIP that has been employed for stimuli-responsive adhesives is poly(benzyl ether)s (PBEs). For example, self-immolative PBE cross-linkers have been designed to produce adhesive thermosets that trigger de-bonding *via* depolymerization;[36] in parallel, the functionalization of PBEs with triazolium-based moieties has achieved competitive

[a]*School of Polymer Science and Engineering, Chonnam National University, 77 Yongbong-ro, Buk-gu, Gwangju 61186, Korea. E-mail: kimhw@jnu.ac.kr*

[b]*School of Mechanical Engineering, Chonnam National University, 77 Yongbong-ro, Buk-gu, Gwangju 61186, Korea*

[c]*Korea Institute of Medical Microrobotics (KIMIRo), Gwangju 61011, Korea*

adhesion strength with various substrates.[37] However, the PBE-based adhesives introduced to date are not reusable and/or demand large quantities of materials given their laborious synthetic process. Notwithstanding, the sophisticated engineering of the macromolecular structure of SIPs has the potential to produce adhesives with the desired features and to dramatically reverse their adhesive performance even in small amounts.

In the present study, we demonstrate the concept for the molecular design for a stimuli-responsive adhesive that is both reusable and de-bondable on demand. To achieve this, self-immolative PBE macro-monomers are designed that are incorporated into a thermally stable, soft polynorbornene matrix via the grafting-through method. Many reactive pendants are pre-positioned on each side chain to provide multiple reversible cross-linking points for the graft copolymer, while head-to-tail depolymerization of the grafted chain cleaves all cross-links at once when triggered by a specific stimulus, leaving only the non-adhesive backbones. The use of only 0.1 mol% PBE leads to the fabrication of a functional thermoset with an adhesive performance similar to high-shear pressure-sensitive adhesives that further can be used in water. The designed material is reusable when exposed to heat but irreversibly and completely de-bondable when no longer needed due to the presence of the remnants of the functional grafts.

The conceptual design of the proposed adhesive thermoset is outlined in Fig. 1. The primary unit of the proposed material is functional PBE branches grafted onto a thermally stable polynorbornene backbone. These branches are self-immolative, with the entire chain depolymerizing inward from the initially triggered unit in response to a specific stimulus. At the same time, tethering units that are embedded in the side chains provide reversible cross-linking points in conjunction with cross-linkers, creating a network structure. The adhesive is thus produced by cross-linking the polynorbornene-*graft*-PBE units.

The polynorbornene backbone with *n*-decyl groups confers elasticity on the copolymer, while the accessible furyl units dangling on the branches allow for the formation of an adhesive network via heating in the presence of a bismaleimide. Due to the nature of the Diels–Alder reaction, the thermoset is thermally reprocessable via covalent bond exchange. Furthermore, the head-to-tail depolymerization of the side chain leads to the cleavage of multiple cross-links as well as the release of repeat units when a single triggering event occurs, resulting in the rapid on-demand de-bonding of the adhesive. Then, the network is converted to linear polynorbornene chains.

Scheme 1 describes the synthetic process for the functional thermoset (**13**). The self-immolative PBE-based macro-monomer (**9**) provides reversible cross-linking points and is degradable in response to a specific stimulus. In this design, a functional initiator (**3**) was synthesized that contains a phenol unit for the initiation of anionic polymerization and a norbornene unit for subsequent grafting-through polymerization. Two types of quinone methide monomer (**7** and **8**) were also synthesized, which contain a lyophilic *n*-butyl side chain and

Fig. 1 Depiction of a stimuli-responsive adhesive thermoset that is both reusable upon heating and de-bondable via induced depolymerization. The thermoset is molecularly designed using functional copolymers that consist of self-immolative and cross-linkable poly(benzyl ether) branches and a thermally stable backbone.
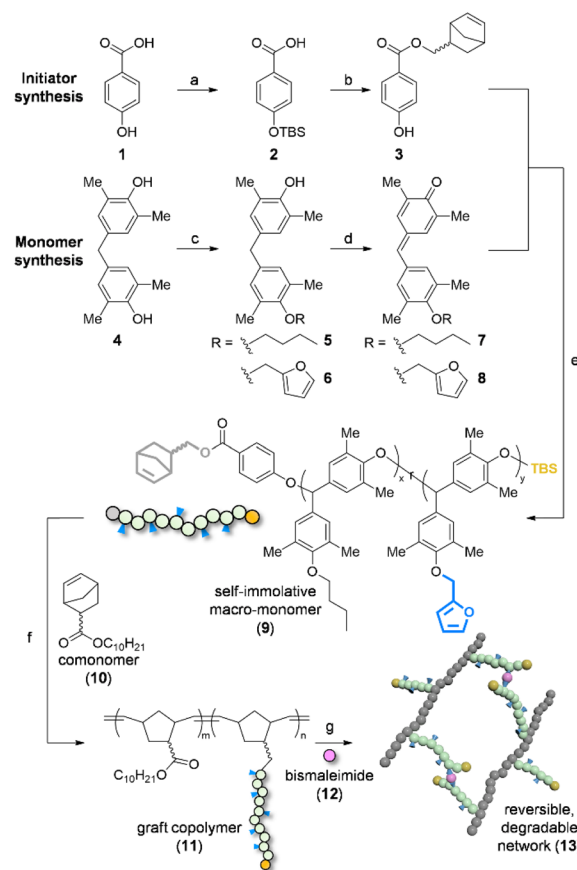
Scheme 1 Synthetic process for the reversible and degradable networks. Reagents and conditions: (a) (i) TBSCl, imidazole; (ii) AcOH (70% over two steps); (b) (i) DCC, DMAP, 5-norbornene-2-methanol; (ii) TBAF (20% over two steps); (c) bromide, K_2CO_3 (70% for **5**; 64% for **6**); (d) Ag_2O (74% for **7**; 62% for **8**); (e) DBU, TBSCl, imidazole (94%); (f) Grubb's 2nd gen. cat., ethyl vinyl ether (66–75%); (g) heat, quantitative. TBS = *tert*-butyldimethylsilyl.

This journal is © The Royal Society of Chemistry 2023

J. Mater. Chem. A, 2023, **11**, 10538–10544 | **10539**

a reactive furyl pendant, respectively. Both monomers were copolymerized at a 1 : 1 molar ratio using **3** (0.1 mol%) in the presence of a base to obtain the statistical copolymer **9**. Its molecular weight was measured to be 27 kDa (*Đ*, 1.29) using gel permeation chromatography (GPC). The 1 : 1 incorporation of the monomers was confirmed based on the OCH$_2$ protons from **7** and **8**, which appeared at 3.72 and 4.74 ppm, respectively, in proton nuclear magnetic resonance (^{1}H NMR) spectroscopic analysis.

Using the norbornene end-group, the designed **9** was then polymerized with comonomer **10** *via* ring-opening metathesis polymerization (ROMP), leading to the formation of graft copolymer **11**. Only 0.1 mol% **9** (*i.e.*, 8.8 wt% with respect to **11**) was used because the steric effect caused by the macro-monomer markedly affected the grafting reaction. For example, employing 1 mol% **9** led to a bimodal distribution in the GPC chromatogram, revealing the presence of both **11** (52%) and unused **9** (48%). In contrast, an almost unimodal distribution of **11** was observed with 0.1 mol% or 0.05 mol% **9**, with negligible amounts of **9** remaining (Fig. S1a†). Meanwhile, the ungrafted **9** in **11** was further quantified using a calibration curve obtained by UV-vis spectrometry. After dispersing **11** in acetone, the unreacted **9** dissolved was analysed based on its absorption peak at 270 nm (Fig. S1b†), which corresponds to merely 0.02 mol% of its feed amount and supports structural integrity of **11**. The molecular weight of **11** increased significantly to 273 kDa, 8.8 times higher than **9**. The statistical incorporation of **9** and **10** was confirmed using NMR based on the proton peaks for OC$\underline{H}$(Ph)$_2$ in **9** (5.53 ppm) and OC$\underline{H}_2$ in **10** (3.99 ppm) (Fig. S3†). The resulting **11** was relatively malleable and resilient compared with the powdery **9** because of the comonomer and its high molecular weight. The furyl groups dangling on the grafts resulted in a cross-linked network with 4,4′-bismaleimidodiphenylmethane (**12**) embedded in the stoichiometry of the reaction sites (*i.e.*, 1 : 1 furan/maleimide) *via* the thermally reversible Diels–Alder reaction. As a result, the elastic, adhesive, brownish **13** was obtained after heating at 120 °C for 4 h.

Due to the cross-linked structure, **13** was more thermally stable up to 370 °C (its 10% weight loss temperature [T_{d10}] obtained from thermogravimetric analysis), with a T_{d10} for **11** of 250 °C. No thermal transition appeared before degradation when monitored using differential scanning calorimetry (Fig. S4†). The gel content of **13** was also found to be sufficiently high to support the covalent cross-linking reaction (Table S1†). Fig. 2a presents the self-immolative behavior of the PBE grafts in response to fluoride. Following a single cleavage event in the TBS group, all repeating units along the backbone sequentially depolymerize *via* repetitive elimination reactions. The head-to-tail depolymerization of PBE occurs autonomously and completely throughout the backbone, producing quinone methide monomers.[29,38]

We investigated the depolymerization behavior of **9** using GPC measurements (Fig. 2b). After exposure to 2.0 equiv. tetra-*n*-butylammonium fluoride (TBAF) in DCM for 1 h, the peak for **9** at the retention time of 14.3 min totally disappeared while new peaks ascribed to the monomer products appeared after 18 min. The feed monomers **7** and **8** after depolymerization were subsequently identified using high-resolution mass spectrometry (Fig. S2†). We also depolymerized the graft copolymer under similar conditions and isolated the resultant polymer by precipitation. The peak in the GPC chromatogram shifted slightly but noticeably (Fig. 2c), and the molecular weight decreased by 30% (*i.e.*, 160 kDa), with a slightly higher dispersity after depolymerization. In addition, the complete removal of the PBE grafts from the polynorbornene backbone was confirmed using the NMR spectroscopy (Fig. S3†). These results demonstrate that the PBE grafts can depolymerize completely even when embedded in other polymeric structures.

Fig. 2d presents control polymers **14**, **15**, and **16**, which were synthesized to demonstrate our design concept. The control macro-monomer **14** was prepared from **7** only in the absence of the furyl pendants. The molecular weight of **14** was found to be 1.6 times higher than that of **9**, which was attributed to its enhanced solubility. Similarly, the control graft copolymer **15** containing 0.1 mol% **14** had a molecular weight that is 15% higher than **11**. Comparison with **16**, which is a high-molecular-weight homopolymer prepared from **10** following a previously reported manner,[36] confirmed that the incorporation of macro-monomers hindered the overall propagation of polynorbornene chains during ROMP, presumably due to the steric effect induced by the macro-monomers. The measured molecular weights and dispersity for these polymers are summarized in Fig. 2e.

The adhesive thermoset **13** was prepared *via* the stoichiometric Diels–Alder reaction between the multifunctional **11** and the bismaleimide **12** as shown in Fig. 3a, with the chemical structure of the resulting reversible cross-linking point presented on the right. The adhesive properties of **13** were studied using lap shear and 180° peel tests (Fig. 3b). As presented in Fig. 3c, pristine **11** had a lap shear strength as low as 0.08 ± 0.01 MPa after heating without **12**. Meanwhile, a mixture of **11** and **12** similarly showed low strengths without heating, which was yet dramatically increasing by 225% after heating. These reveal the network formation is essential to cause adhesive properties of **13** rather than the presence of **12** *per se*. The strength of **13** was 0.25 ± 0.01 MPa, 25 times as high as that of double-sided tape. After heating them in the presence of **12**, the controls **15** and **16** without furan moieties exhibited a similar strength to **11**, owing to the lack of the covalent cross-linking. A similar trend was found in the results for the peel test, with the peel strength of **13** twice as high as that of commercial tape. Given the results above, the adhesive performance of **13** is considered to be basically caused from the polynorbornene with decyl side chains owing to non-covalent electrostatic interactions such as dispersion force, which is then significantly enhanced after post-thermal cross-linking. Representative data obtained from both tests are presented in Fig. S5.†

Swapping the cross-linker altered the adhesive properties of the entire network (Fig. 3d). The relatively short **17** or the bent **18** were used to replace **12** in forming a network with **11**. With **17**, the lap shear and peel strength decreased by 16% and 24%, respectively, compared with **13**. With **18**, a greater decrease in the strength was observed, which was similar to that of **11**

10540 | *J. Mater. Chem. A*, 2023, **11**, 10538–10544

This journal is © The Royal Society of Chemistry 2023
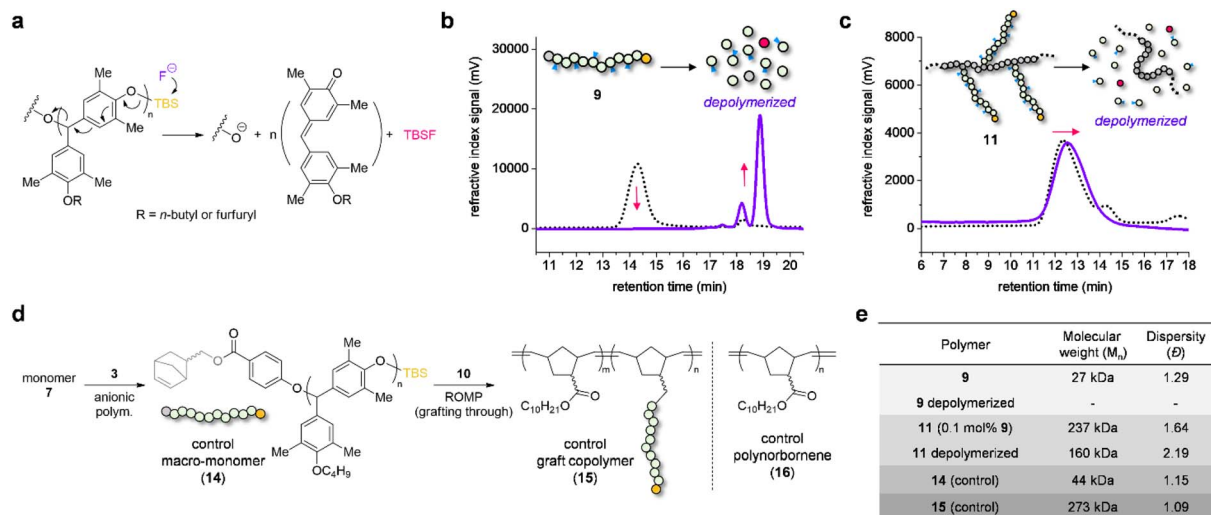
Fig. 2 (a–c) Designed depolymerization behavior of the graft copolymer **11**. (a) The reaction mechanism for the head-to-tail depolymerization of the polymer grafts of **9** in response to fluoride; TBS = *tert*-butyldimethylsilyl. (b and c) GPC chromatograms of as-prepared (dotted black) (b) **9** and (c) **11** and after exposure to fluoride (violet). Illustrations of the depolymerization of **9** and **11** are presented in the insets. (d) Synthetic process for the control macro-monomer **14** without furfuryl units and the resulting graft copolymer **15**. Control polymer **16** without the polymer grafts is shown on the right. (e) Summary of the molecular weight and dispersity obtained for all polymers.

without **12**. Considering mechanical properties of thermosets are affected by cross-linking density, the short or bent cross-linkers were deemed not to provide sufficient inter-chain cross-linking of **11**, probably due to reduced accessibility of the maleimides toward the dangling furans, as found before.[39] Representative data are shown in Fig. S6.†

The viscoelastic behavior of **13** was investigated using dynamic mechanical analysis (DMA) to quantify its adhesive properties (Fig. 3e). In frequency sweep mode, the storage and
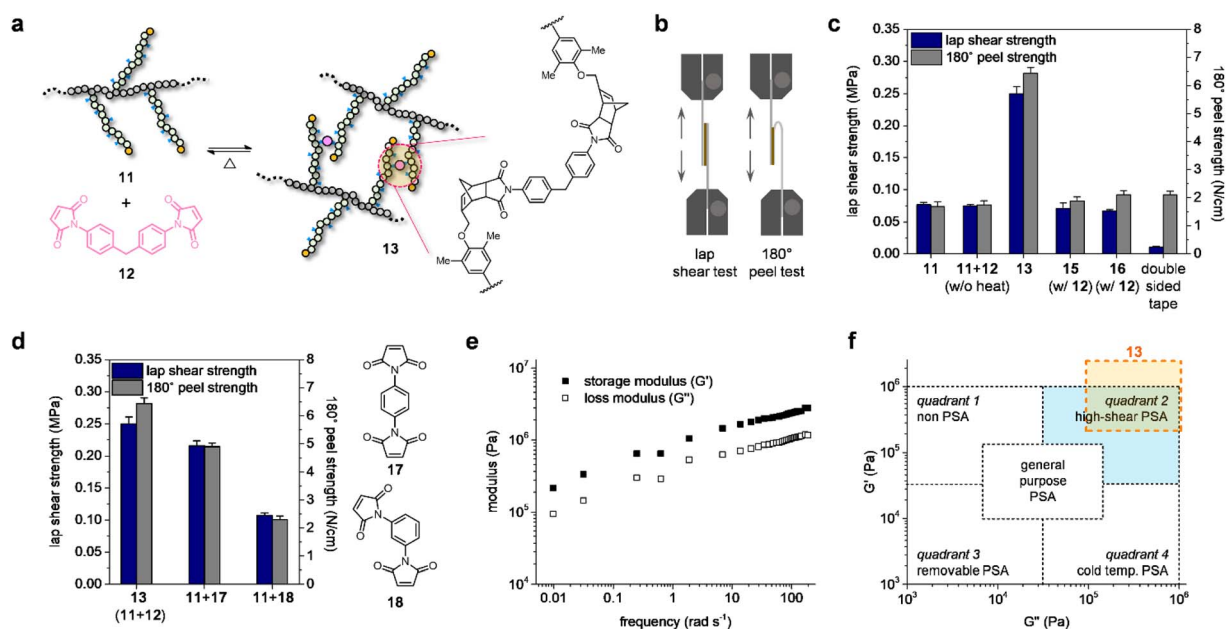
Fig. 3 Formation of the adhesive thermoset **13** *via* thermal treatment and experimental data for its adhesive properties. (a) Illustration of the thermally reversible cross-linking process for **11** in the presence of **12**. Chemical structure of the cross-linking point is shown on the right. (b) Diagrams of the lap shear and 180° peel tests conducted on the materials. (c) The lap shear strength (navy) and the peel strength (gray) obtained from the materials. The values for commercial double-sided tape are presented for comparison. (d) The effect of cross-linkers on the adhesive properties of the resulting networks (lap shear test, navy; 180° peel test, gray). The chemical structures of the control bismaleimides (**17** and **18**) are presented on the right. (e) Changes in the storage and loss moduli (G' and G'', respectively) of **13** with an increase in the frequency at 25 °C. (f) Viscoelastic window for **13** (orange region) in comparison with Chang's criteria for pressure-sensitive adhesives.

loss moduli (G' and G'', respectively) of **13** increased with an increase in frequency, and the loss factor was estimated to be <1 over the tested frequency range (Fig. S7†). These results confirmed the predominant elastic nature of the network. Of particular note is that both dynamic moduli measured at 0.01 and 100 rad s^{-1} give the impress of pressure-sensitive adhesive (PSA), each of which indicates the bonding and de-bonding frequency of PSAs.[40] The G' at the bonding frequency of **13** meets the Dahlquist criterion ($G' < 3.3 \times 10^5$ Pa),[41] and its viscoelastic window falls in quadrant 2 as classified by Chang.[42] Based on these two benchmarks, **13** can be classified for use as a high-shear PSA. Given that the viscoelastic window depends on the moduli, various types of PSA could be fabricated using **13** by adjusting the molar ratio of the components or the molecular weight of **9**. In fact, the adhesive strength of **13** is lower than that of other polynorbornene-based materials that are cross-linked with PBE-based additives.[36] Nonetheless, here we are able to achieve the chemically defined thermosets using PBE-based monomers and further demonstrate them as a functional PSA.

Following our design principles, the adhesive **13** is not only healable when damaged but also de-bondable when no longer needed. As shown in Fig. 4a, this reusability originates from the reversible bond exchange when heated, while the degradability is the result of depolymerization.

The impact of the bond exchange was demonstrated by re-bonding the damaged samples *via* thermal treatment (Fig. 4b). After the glued glass slides were detached by force, they could no longer be glued together, with a measured lap sheer strength of only 0.02 ± 0.01 MPa. This would be ascribed to cohesive failure of **13** that occurred along with adhesive failure (Fig. S8a†). So, chain entanglement could not be fully restored and separate adherends could be roughened during dismantlement, which hinders the recovery of the adhesion at room temperature. However, this increased to 0.14 ± 0.01 MPa when the adhesive was heated at 80 °C for 4 h, before returning to its initial value after heating at 120 °C for the same period of time. Representative load–displacement curves for the adhesive samples are presented in Fig. S8b.† In addition, we observed a similar lap shear strength for each of four repeating detachment–re-attachment cycles, thus verifying the reusability of **13** (Fig. 4b). Restoring the adhesive properties of the de-bonded material was temperature-dependent, with thermal treatment at 120 °C sufficient for the retro-Diels–Alder reaction, which led to the topological re-arrangement of the Diels–Alder linkage when cooled to room temperature. Further, the thermo-reversible bonding behavior of the adhesive was confirmed using peel tests, with the peel strength after detachment recovering completely after heating at 120 °C (Fig. S8c†).

On the other hand, the glass slides glued using **13** were able to be separated in the presence of fluoride. Exposure to 100 mM TBAF under aqueous conditions at 25 °C immediately led to an exponential decrease in the lap shear strength, with complete de-bonding occurring within 9 h due to the depolymerization of **13**. We also examined the effect of the fluoride concentration on the triggered de-bonding behavior, with lower concentrations requiring a longer induction period in the initial stage, after
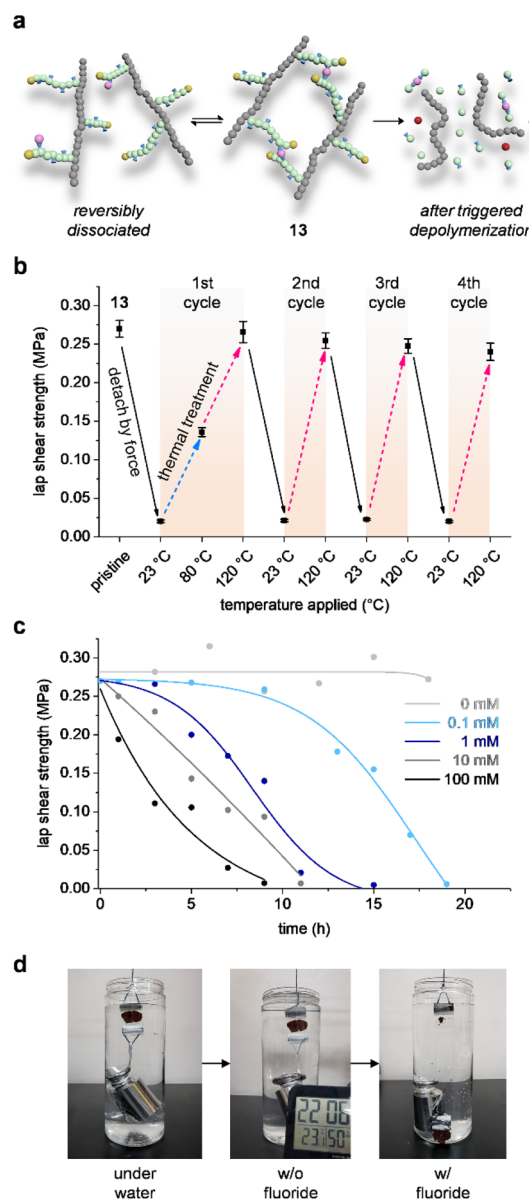
Fig. 4 (a) Schematic description for the structural change induced in **13** when reversibly dissociated or irreversibly depolymerized. (b) Reversible change in the lap shear strength of **13** when detached by force (solid) and that after being restored by thermal treatment (dotted). Four detachment–reattachment cycles are presented. (c) Irreversible change in the lap shear strength of **13** when exposed to different concentrations of fluoride (0–100 mM in 1 : 1 water–ethanol, v/v) at 25 °C. (d) Photographs for underwater adhesion of **13** holding a 3 kg weight: (left) as-prepared, (middle) after storage for a day in the absence of fluoride, and (right) upon the addition of fluoride (5 mM) at room temperature.

which a similar decrease in the adhesion strength was observed. For example, with 0.1 mM fluoride, the induction period was 10 h, after which a decrease in the strength was observed for 9 h until de-bonding, as was the case with a concentration of 100 mM. These results indicate that, once initiated, the head-to-tail depolymerization of **13** leads to the de-bonding of adhesives irrespective of the degree to which the stimulus is supplied.

10542 | *J. Mater. Chem. A*, 2023, **11**, 10538–10544

This journal is © The Royal Society of Chemistry 2023

Without fluoride, **13** maintained a constant strength over the experimental period, as expected (Fig. 4c). The load–displacement curves for the samples recorded during the lap shear tests are presented in Fig. S9.†

The de-bondable underwater adhesion of **13** was also demonstrated in a large-scale test (Fig. 4d). Glass slides (2.5 × 1.2 cm^2) glued together using **13** were able to hold a 3 kg weight underwater for a day at room temperature. However, as soon as a small amount of 1 M TBAF solution was added, the joint came apart and the weight fell. Due to the presence of the weight, a fluoride concentration as low as 5 mM resulted in the rapid de-bonding of the glass slides.

Conclusions

In conclusion, we demonstrated the molecular design of a reusable and de-bondable adhesive thermoset. To achieve this, self-immolative macro-monomers were synthesized *via* anionic polymerization using two types of quinone methide monomer and a functional initiator. A polynorbornene-*graft*-PBE copolymer was then fabricated *via* grafting-through polymerization. Each PBE branch on the polynorbornene backbone provided multiple, reversible cross-linking points and entirely depolymerizes when exposed to a single triggering event. Elastic networks were thus obtained after thermal treatment in the presence of cross-linkers. These were then used as a high-shear pressure-sensitive adhesive and subjected to lap shear and peel tests, exhibiting an adhesive strength that is higher than that of general adhesive tape. As designed, the adhesive could also be restored when damaged due to reversible covalent bond exchange, while rapid de-bonding on demand was possible due to the instant cleavage of multiple cross-links *via* head-to-tail depolymerization. It is believed that the adhesive strength can be optimized by adjusting the feed ratio or molecular weight of the components and employing other end-caps rather than TBS can allow to use various stimuli such as pH, enzyme, heat or light that are eco-friendly or further provide a spatiotemporal control of adhesives.[43,44] In addition, our conceptual design can be advanced with the use of various comonomers and bio-inspired responses, allowing its use in a variety of industrial and biomedical applications.

Conflicts of interest

There are no conflicts to declare.

Acknowledgements

Notes and references

1 N. D. Blelloch, H. J. Yarbrough and K. A. Mirica, *Chem. Sci.*, 2021, **12**, 15183–15205.
2 A. Hutchinson, Y. Liu and Y. Lu, *J. Adhes.*, 2017, **93**, 737–755.
3 C. Creton and E. Papon, *MRS Bull.*, 2003, **28**, 419–421.
4 J. C. Yang, J. Mun, S. Y. Kwon, S. Park, Z. Bao and S. Park, *Adv. Mater.*, 2019, **31**, 1904765.
5 Y. U. Cho, S. L. Lim, J.-H. Hong and K. J. Yu, *npj Flexible Electron.*, 2022, **6**, 53.
6 N. D. A. Watuthanthrige, D. Dunn, M. Dolan, J. L. Sparks, Z. Ye, M. B. Zanjani and D. Konkolewicz, *ACS Appl. Polym. Mater.*, 2022, **4**, 1475–1486.
7 Y. Jin, Z. Wang, C. Hu, J. Wang, K. Yan, J. He, Z. Wang, Z. Wang and L. Yuan, *Green Chem.*, 2023, **25**, 1157–1168.
8 Q. Zhao, M. Zhang, S. Gao, Z. Pan, Y. Xue, P. Jia, C. Bo, Z. Luo, F. Song and Y. Zhou, *J. Mater. Chem. A*, 2022, **10**, 11363–11374.
9 C. Cui, X. Chen, L. Ma, Q. Zhong, Z. Li, A. Mariappan, Q. Zhang, Y. Cheng, G. He, X. Chen, Z. Dong, L. An and Y. Zhang, *ACS Appl. Mater. Interfaces*, 2020, **12**, 47975–47983.
10 W. Liu, C. Fang, F. Chen and X. Qiu, *ChemSusChem*, 2020, **13**, 4691–4701.
11 D. Santiago, D. Guzmán, J. Padilla, P. Verdugo, S. D. Flor and À. Serra, *ACS Appl. Polym. Mater.*, 2023, **5**, 2006–2015.
12 C. Li, Y. Chen, Y. Zeng, Y. Wu, W. Liu and R. Qiu, *Eur. Polym. J.*, 2022, **162**, 110923.
13 J. Zhou, L. Wang, L. Li and S. Feng, *Polym. Chem.*, 2020, **11**, 4780–4786.
14 Z. Zhou, X. Su, J. Liu and R. Liu, *ACS Appl. Polym. Mater.*, 2020, **2**, 5716–5725.
15 Y. Oh, J. Park, J.-J. Park, S. Jeong and H. Kim, *Chem. Mater.*, 2020, **32**, 6384–6391.
16 F. Ji, X. Liu, D. Sheng and Y. Yang, *Polymer*, 2020, **197**, 122514.
17 P. S. Roy, M. M. Mention, A. F. Patti, G. Garnier, F. Allais and K. Satio, *Polym. Chem.*, 2023, **14**, 913–924.
18 M. Aizawa, H. Akiyama, T. Yamamoto and Y. Matsuzawa, *Langmuir*, 2023, **39**, 2771–2778.
19 Y. Zhou, M. Chen, Q. Ban, Z. Zhang, S. Shuang, K. Koynov, H.-J. Butt and S. Wu, *ACS Macro Lett.*, 2019, **8**, 968–972.
20 S. H. Jung, G. Choi, S. Jeong, J. Park, H. Yoon, J.-J. Park and H. Kim, *ACS Sustainable Chem. Eng.*, 2022, **10**, 13816–13824.
21 T. S. Babra, C. Warriner, N. Bazin, W. Hayes and B. W. Greenland, *Mater. Today Commun.*, 2021, **26**, 101777.
22 B. R. Freedman, O. Uzun, N. M. M. Luna, A. Rock, C. Clifford, E. Stoler, G. Östlund-Sholars, C. Johnson and D. J. Mooney, *Adv. Mater.*, 2021, **33**, 2008553.
23 H. Yang, C. Li, J. Tang and Z. Suo, *ACS Appl. Bio Mater.*, 2019, **2**, 1781–1786.
24 A. Badía, M. J. Barandiaran and J. R. Leiza, *Eur. Polym. J.*, 2021, **144**, 110244.
25 C. Liu, X. Xie, X. kong, Q. Zhang, J. Yang, J. Yang and W. Wang, *Mater. Lett.*, 2022, **316**, 132019.
26 J. Tan, J. Hu and S. Liu, *Polym. Chem.*, 2021, **12**, 6230–6241.
27 S. Wang and M. W. Urban, *Nat. Rev. Mater.*, 2020, **5**, 562–583.
28 L. M. de Espinosa, W. Meesorn, D. Moatsou and C. Weder, *Chem. Rev.*, 2017, **117**, 12851–12892.
29 O. Shelef, S. Gnaim and D. Shabat, *J. Am. Chem. Soc.*, 2021, **143**, 21177–21188.

This journal is © The Royal Society of Chemistry 2023

J. Mater. Chem. A, 2023, **11**, 10538–10544 | **10543**

30 A. G. Gavriel, M. R. Sambrook, A. T. Russell and W. Hayes, *Polym. Chem.*, 2022, **13**, 3188–3269.

31 R. E. Yardley, A. R. Kenaree and E. R. Gillies, *Macromolecules*, 2019, **52**, 6342–6360.

32 H. Kim, A. D. Brooks, A. M. DiLauro and S. T. Phillips, *J. Am. Chem. Soc.*, 2020, **142**, 9447–9452.

33 D. Jung, K. M. Lee, T. Tojo, Y. Oh, H. Yoon and H. Kim, *Chem. Mater.*, 2019, **31**, 6249–6256.

34 Y. Xiao, X. Tan, Z. Li and K. Zhang, *J. Mater. Chem. B*, 2020, **8**, 6697–6709.

35 Q. E. A. Sirianni and E. R. Gillies, *Polymer*, 2020, **202**, 122638.

36 H. Kim, H. Mohapatra and S. T. Phillips, *Angew. Chem., Int. Ed.*, 2015, **54**, 13063–13067.

37 Z. Cheng, G. Zheng, Z. Tian, X. Chao, Y. Xiao, J. Li and Y. Bai, *ACS Appl. Polym. Mater.*, 2022, **4**, 6812–6816.

38 J. W. Kim, H. J. Kim, J. Park, J. A. Chae, H.-W. Song, E. Choi and H. Kim, *Macromolecules*, 2022, **55**, 6140–6149.

39 Q. Zhou, Z. Sang, K. K. Rajagopalan, Y. Sliozberg, F. Gardea and S. A. Sukhishvili, *Macromolecules*, 2021, **54**, 10510–10519.

40 T. T. D. Chen, L. P. Carrodeguas, G. S. Sulley, G. L. Gregory and C. K. Williams, *Angew. Chem., Int. Ed.*, 2020, **59**, 23450–23455.

41 C. A. Dahlquist, in *Treatise on Adhesion and Adhesives*, ed. R. L. Patrick, Marcel Dekker, New York, 1969, vol. 2, pp. 219–260.

42 E. P. Chang, *J. Adhes.*, 1991, **34**, 189–200.

43 D.-G. Cho and J. L. Sessler, *Chem. Soc. Rev.*, 2009, **38**, 1647–1662.

44 M. E. Roth, O. Green, S. Gnaim and D. Shabat, *Chem. Rev.*, 2016, **116**, 1309–1352.

10544 | *J. Mater. Chem. A*, 2023, **11**, 10538–10544

This journal is © The Royal Society of Chemistry 2023